Journal of Holography Applications in Physics
Volume 6, Issue 1, Winter 2026, 98–125
©Available online at http://jhap.du.ac.ir
DOI: 10.22128/jhap.2025.3126.1156
Online ISSN: 2783–3518

Regular article

Holographic and Thermodynamic Topological Perspectives on AdS Einstein–Power–Yang–Mills Black Holes with Generalized Entropy

N. Ramya[1] · R. Tamilamuthan[2] · Hossein Rashmanlou[3] · Farshid Mofidnakhaei[4]

[1] Department of Mathematics, Kongu Engineering College, Erode-638060, India; Corresponding Author E-mail: jpramyamaths@gmail.com

[2] Department of Electrical and Electronics Engineering, Assistant Professor, PERI Institute Of Technology, Chennai-600048, India.
E-mail: tamilamuthan.rdg@gmail.com

[3] Canadian Quantum Research Center, 106-460 Doyle Ave, Kelowna, British Columbia V1Y 0C2 Canada.
E-mail: Rashmanlou.1987@gmail.com

[4] Department of Physics, Sar. C., Islamic Azad University, Sari, Iran.
E-mail:Farshid.Mofidnakhaei@gmail.com

Received: November 4, 2025; **Revised:** November 16, 2025; **Accepted:** December 8, 2025

Abstract. In this work, we explore the holographic and thermodynamic topology of Anti–de Sitter (AdS) Einstein–Power–Yang–Mills (EPYM) black holes using both the bulk–boundary correspondence and the restricted phase space (RPS) frameworks. The study employs several non-extensive entropy models, including Barrow, Rényi, Sharma–Mittal, Kaniadakis, and Tsallis–Cirto entropies. Within the bulk–boundary formalism, we find that the free deformation parameters strongly influence the classification of topological charges w. For the Barrow entropy, two distinct topological charges $w = +1$ and $w = -1$ appear as the deformation parameter increases, closely resembling the Bekenstein–Hawking limit. The Rényi entropy exhibits a transition from three charges $w = (+1, 0, -1)$ to a single charge $w = +1$ as the non-extensive parameter rises, while setting the deformation parameter to zero yields two symmetric charges $w = \pm 1$. In the Sharma–Mittal framework, three characteristic regions emerge: for higher parameter ratios, $w = +1$; for balanced ratios, $w = 0$; and for lower ratios, $w = -1$. The Kaniadakis entropy generally shows $w = \pm 1$ for most admissible K values, except at $K = 0$, where only $w = +1$ remains. The Tsallis–Cirto entropy displays two topological charges $w = \pm 1$ for small deformation parameters and a single charge $w = +1$ as the parameter approaches 0.9. Extending the analysis to the RPS framework reveals that, for Rényi, Sharma–Mittal, and Tsallis–Cirto entropies, the topological charge remains invariant at $w = +1$, regardless of parameter variation. However, in the Barrow and Kaniadakis cases, the topological configuration evolves with increasing non-extensivity, leading to distinct topological transitions in w. These findings provide deeper insights into the holographic and thermodynamic structure of non-extensive AdS black holes and highlight their phase evolution under generalized entropy formulations. The present work differs by (i) an explicit bulk→boundary holographic mapping that tracks how the EPYM power q modifies boundary central-charge and chemical potential variables, (ii) additional analytic expansions and parameter-range scans for q and entropy deformation parameters, and (iii) the introduction of supplementary stability diagnostics and response-function tests that probe the robustness of the topology classification.

Keywords: Holography; Thermodynamic; Black holes; Topology.

Contents

1 Introduction

The thermodynamic behavior of black holes provides a fundamental link between general relativity, quantum mechanics, and statistical physics. Gashti et al. [1] explored the phase-space structure and thermodynamic topology of AdS black holes under a non-extensive entropy framework, examining both bulk and boundary correspondences and highlighting how deviations from classical entropy formulations reshape topological classifications of black hole phases. Building on this, Gashti and Pourhassan [2] extended the analysis by integrating holographic thermodynamics with non-extensive statistics, demonstrating that topological invariants provide refined insight into holographic dualities and stability regimes of black holes.

Soroushfar et al. [3] connected geodesic motion with thermodynamic quantities in Einstein–Power–Yang–Mills AdS black holes, revealing how spacetime curvature directly influences thermodynamic geometry, whereas Bellucci and Tiwari [4] earlier demonstrated that the curvature of thermodynamic space encapsulates microscopic interactions and phase transitions in Einstein–Yang–Mills black holes. Hu et al. [5] further studied holographic imaging of Einstein–Power–Yang–Mills AdS black holes, showing that critical behavior and horizon topology can be probed holographically. Du et al. [6] examined Barrow-modified entropy in the restricted phase space, uncovering how non-extensive corrections affect thermodynamic quantities and critical exponents.

Rani et al. [7] employed Tsallis entropy to reconstruct black hole thermodynamic geometry, demonstrating that non-additivity significantly influences topological phase classification. Afshar et al. [8] examined black hole thermodynamics from a CFT perspective, finding that non-extensive entropies alter both holographic correspondence and the Euler characteristic of the thermodynamic manifold. Sadeghi et al. [9] provided a unified classification of black holes across bulk–boundary, extended, and restricted phase-space approaches, while Wu and Wei [10] analyzed quantum BTZ black holes, revealing quantum-induced modifications to topological charges. Zafar et al. [11] applied Barrow entropy to black holes with clouds of strings and quintessence, identifying new entropy-driven topological transitions.

Tong et al. [12] explored topological structures via Rényi statistics, whereas Hazarika et al. [13] employed Kaniadakis statistics, illustrating that generalized entropies induce distinct thermodynamic curvature signatures. Gashti et al. [14] showed that loop quantum gravity corrections further deform thermodynamic topological classification. Hazarika and Phukon [15] addressed the restricted phase-space topology of Kerr–Sen–AdS black holes, emphasizing the sensitivity of topological invariants to entropy deformations. Zhang and Jiang [16] discussed bulk–boundary thermodynamic equivalence from a topological viewpoint, and Jawad and Fatima [17] confirmed that Barrow entropy modulates phase transition structures in charged AdS black holes.

Promsiri et al. [18] investigated Van der Waals-like transitions in charged flat-space black holes via Rényi entropy, while Shahzad et al. [19] examined dyonic AdS black holes in Einstein–Gauss–Bonnet gravity, highlighting higher-dimensional effects on topological indices. Capozziello and Shokri [20] analyzed Barrow entropy within AdS thermodynamics, reaffirming its compatibility with modified gravity. Wu and Wu [21] classified rotating AdS black holes through topological invariants, whereas Sekhmani et al. [22] studied 5D AdS black holes under Kaniadakis statistics, demonstrating entropy-dependent phase structures. Ladghami et al. [23] contextualized Barrow entropy within restricted phase-space thermodynamics, bridging non-extensive and AdS formulations.

Tsallis [24] revisited black hole entropy through his non-extensive statistical framework, arguing that long-range correlations and non-additive behavior necessitate a departure from

Boltzmann–Gibbs entropy for gravitational systems. Brzo et al. [25] analyzed AdS black holes under non-commutative geometry and Barrow entropy, showing that the combination of fractal corrections and spacetime non-commutativity generates deformed topological structures, shifts critical points, and introduces new stability regimes. Luciano and Saridakis [26] investigated the effect of Kaniadakis entropy on PV criticality and phase transitions, revealing distinct geometric-thermodynamic signatures.

Ramya and Deivanayaki [27] analyzed the impact of microorganisms on Carreau nanofluid flow within a Darcy–Forchheimer porous medium under magnetohydrodynamic effects. Their findings revealed that the interaction between nonlinear viscosity, porous resistance, and bioconvective forces significantly modifies both the momentum and mass transfer characteristics, demonstrating enhanced thermal–solutal coupling due to microbial activity.

Ramya and Deivanayaki [28] numerically examined Casson micropolar fluid flow over an inclined porous surface, highlighting how micropolar rotation and Casson rheology influence shear stress, velocity gradients, and heat transfer. The study underscored the crucial role of inclination and porous resistance in controlling boundary layer thickness and energy transport.

Ramya et al. [29] investigated micropolar nanofluid flow over an exponentially stretching surface subjected to homogeneous–heterogeneous chemical reactions and the Cattaneo–Christov heat flux model. Their analysis demonstrated that non-Fourier heat conduction and reaction coupling markedly affect temperature and concentration fields, providing a more realistic description of heat transport in reactive nanofluid systems.

Muhiuddin et al. [30] performed a detailed thermal and bioconvective study of Williamson fluid flow over a porous curved stretching surface considering homogeneous–heterogeneous reactions. The results showed that curvature and porous resistance profoundly influence the fluid's bioconvective stability and heat transfer, bridging the gap between non-Newtonian rheology and microbial transport phenomena.

Ramya et al. [31] examined the combined effects of thermophoresis and Brownian motion on Casson ternary hybrid nanofluid flow containing gyrotactic microorganisms over a horizontal plate. Their work highlighted the dual role of nanoparticle migration and microbial motility in enhancing heat and mass transfer, offering novel insights into the coupled dynamics of hybrid nanofluid–bioconvective systems.

Sadeghi et al. [32] analyzed Bardeen black hole thermodynamics from a topological standpoint, illustrating that the regularity of spacetime modifies the topological charge and phase transition structure. Chen and Wei [33] explored the thermodynamic topology of dyonic AdS black holes featuring multiple defect curves, revealing that these defects induce intricate topological transitions in the extended phase space. Myung et al. [34] investigated the thermodynamics of regular black holes, showing that introducing a finite core removes singularities and leads to a modified phase structure. Liu and Wang [35] examined the topological nature of Gauss–Bonnet AdS black holes, demonstrating that higher-order curvature corrections alter the topological charge and critical behavior.

Barrow [36] introduced the concept of fractal or rough black hole horizons, proposing Barrow entropy as a non-extensive modification of the Bekenstein–Hawking law. Kaniadakis [37] developed a relativistic generalization of statistical mechanics, providing a consistent entropy measure for relativistic and gravitational systems. Rényi [38] introduced a generalized entropy measure extending Shannon entropy to non-extensive systems, while Sharma and Mittal [39] proposed a two-parameter non-additive entropy formulation unifying Tsallis and Rényi frameworks. Tsallis and Cirto [40] later applied Tsallis non-extensive statistics to black hole thermodynamics, linking horizon area scaling to long-range interactions.

Wei, Liu, and Mann [41] initially conceptualized black holes as topological thermodynamic defects, while Wei and Liu [42] formalized the connection between winding numbers

of free-energy curves and stable/unstable phases. Foundational holographic frameworks by Maldacena [43] and Witten [44] confirmed that boundary conformal theories encode bulk gravitational thermodynamics, and Kubizňák et al. [45] introduced black hole chemistry with a variable cosmological constant, laying the groundwork for phase-space topology analyses.

The present study extends this approach by introducing an explicit dependence of the topological charge on the EPYM exponent γ and entropy deformation parameter q, performing a holographic mapping between bulk and boundary thermodynamic variables, and constructing parameter-space heatmaps that reveal previously unreported phase domains. In addition, asymptotic expansions for $q \to 1$ and $q \to 0$ are derived to confirm consistency with the Bekenstein–Hawking limit.

2 Objectives of the Study

The primary objective of this work is to investigate the holographic and thermodynamic topology of AdS EPYM black holes under generalized non-extensive entropy frameworks. By integrating both bulk–boundary correspondence and restricted phase-space (RPS) analyses, this study aims to develop a unified understanding of how nonlinearity in gauge dynamics and entropy deformation collectively influence topological phase structures in AdS black holes. The specific objectives are outlined as follows:

1. To analyze the thermodynamic topology of AdS EPYM black holes using both the bulk–boundary correspondence and RPS formalisms, providing a comparative topological classification across frameworks.

2. To incorporate multiple generalized entropy formulations—Barrow, Rényi, Sharma–Mittal, Kaniadakis, and Tsallis–Cirto—and investigate how their deformation parameters modify the evolution of topological charge w and zero points (ZPs).

3. To examine the influence of key model parameters such as the Yang–Mills power exponent q and entropy deformation parameters δ, λ, (α, β), K, and Δ on the emergence, annihilation, and bifurcation of thermodynamic topological states.

4. To establish the correspondence between changes in topological charge and the stability of black hole phases through holographic and response-function diagnostics, linking winding number transitions with thermodynamic susceptibility.

5. To construct an explicit holographic mapping between bulk deformation parameters and boundary thermodynamic variables, including the boundary central charge and chemical potential, clarifying how bulk non-extensivity manifests in boundary field theory.

6. To perform analytic limit checks and asymptotic expansions of free energy and winding number near $q \to 1$ and $q \to 0$, thereby recovering the Bekenstein–Hawking limit and identifying parameter regimes beyond previous studies.

7. To introduce supplementary stability diagnostics—such as heatmap visualizations in $(q, \text{entropy parameter})$ space and second-derivative response functions in RPS variables—to verify the robustness of topological classifications.

8. To provide a concise computational framework summarizing the numerical workflow and parameter-space exploration that supports reproducibility of all results.

Collectively, these objectives extend the scope of earlier studies such as Gashti and Pourhassan [1,2] by: (i) implementing a direct bulk-to-boundary holographic dictionary for EPYM systems; (ii) performing broader parameter-domain analyses and analytic expansions not previously reported; and (iii) introducing independent stability and response-function diagnostics. Through these additions, the present work establishes a more comprehensive and holographically consistent understanding of the thermodynamic topology and non-extensive phase evolution of AdS EPYM black holes.

Nonlinear Extension in the EPYM Framework

To capture nonlinear effects within the EPYM sector, the standard Yang–Mills invariant $(F_{\mu\nu}F^{\mu\nu})$ is generalized as $(F_{\mu\nu}F^{\mu\nu})^{\gamma}$, where $\gamma > 0$ represents the field-strength exponent. This deformation parameter influences the black-hole equation of state and modifies the topology of the thermodynamic potential. The generalized mass and temperature functions are recalculated as

$$M = M(r_+, q, \gamma), \qquad T = \frac{\partial M}{\partial S}, \tag{2.1}$$

and the free energy is evaluated from $F = M - TS$. The resulting topology is analyzed through its dependence on (S, γ, q).

3 Methodology

The methodological framework of this study combines the principles of thermodynamic topology, non-extensive statistical mechanics, and holographic duality to analyze the AdS EPYM black hole system. The analysis is conducted within two complementary formalisms: (i) the bulk–boundary correspondence, which connects the gravitational dynamics in the bulk spacetime to the thermodynamic behavior on the AdS boundary, and (ii) the restricted phase space (RPS) formalism, which constrains certain thermodynamic variables to establish a consistent topological classification. The methodology adopted in this work is structured as follows.

3.1 Bulk–Boundary Framework

In the bulk–boundary approach, the thermodynamic properties of the AdS EPYM black hole are studied through the metric function [42]

$$f(r) = 1 - \frac{2GM}{r} + \frac{r^2}{l^2} + \frac{G(2q^2)^{\gamma}}{2(4\gamma - 3)r^{4\gamma-2}}, \tag{3.1}$$

where M is the black hole mass, q is the Yang–Mills charge, G is the gravitational constant, l is the AdS radius, and γ is the power-law exponent of the Yang–Mills field. The Hawking temperature associated with the event horizon r_h is given by

$$T = \frac{1 + 8\pi G P r_h^2 - \dfrac{(2q^2)^{\gamma} G}{2r_h^{4\gamma-2}}}{4\pi r_h}, \tag{3.2}$$

and the corresponding black hole mass reads

$$M = \frac{r_h}{2G}\left(1 + 8\pi G P r_h^2 - \frac{(2q^2)^{\gamma} G}{2(4\gamma - 3)r_h^{4\gamma-2}}\right), \tag{3.3}$$

where P denotes the thermodynamic pressure related to the cosmological constant. Using these relations, the Helmholtz free energy $\mathcal{F}$ and Euclidean time period τ are derived for each entropy model. The topological charge w is then determined through Duan's ϕ-mapping method, which associates w with the winding number of the vector field $(\phi^{r_h}, \phi^{\Theta})$ in the τ–Θ plane. This framework enables a direct correspondence between phase transitions and topological structures in the thermodynamic manifold.

In the present analysis, we adopt the phenomenological approach widely used in studies of non-extensive and generalized entropies, in which the black hole geometry is kept fixed while the entropy functional is modified to incorporate statistical or quantum-gravitational corrections. This assumption is justified in the small-deformation regime—where the Rényi index, Barrow parameter δ, Kaniadakis constant K, or Sharma–Mittal ratio α/β are perturbatively small—so that backreaction on the metric and thermodynamic quantities is negligible. Such an effective treatment allows the exploration of how entropy deformation alone alters the thermodynamic topology without solving new field equations. This methodology has been followed in several related works on topological thermodynamics and generalized entropy frameworks (see, e.g., Wei and Liu [42]; Wei, Liu, and Mann [41]; Liu and Wang [35]).

3.2 Restricted Phase Space (RPS) Formalism

The restricted phase space (RPS) formalism provides a complementary perspective in which the AdS radius l and related quantities are held fixed, allowing the thermodynamic quantities to be redefined in terms of the central charge C and rescaled charge $\hat{q}$. The RPS identifications are expressed as

$$q = \frac{\hat{q}}{\sqrt{C}}, \qquad G = \frac{l^2}{C}, \qquad S = \frac{C\pi r_h^2}{l^2}. \tag{3.4}$$

With these definitions, the Hawking temperature becomes

$$T = \frac{1 + \dfrac{r_h^2}{l^2} - \dfrac{(2\hat{q}^2/C)^{\gamma} l^2}{2C r_h^{4\gamma-2}}}{4\pi r_h}. \tag{3.5}$$

The corresponding mass and Gibbs-like heat capacity are then determined, from which the Euclidean time period τ and the ϕ-fields are reconstructed. This allows the computation of the zero points (ZPs) and classification of the associated topological charges ($w = +1, 0, -1$).

4 Thermodynamic Relations for Non-Extensive Entropy Models

In this section, we develop a unified thermodynamic structure for six non-extensive entropy formalisms—Tsallis, Rényi, Sharma–Mittal, Barrow, Kaniadakis, and Tsallis–Cirto—and derive the corresponding effective temperature, first law of thermodynamics, heat capacity, and Smarr relation. We begin with the standard Bekenstein–Hawking entropy

$$S_{BH} = \pi r_+^2, \tag{4.1}$$

and the Hawking temperature

$$T_H = \frac{1}{4\pi r_+}\left(1 + \frac{3r_+^2}{\ell^2}\right). \tag{4.2}$$

For any entropy model $S_{\rm NE}(S_{BH})$, the effective temperature is defined as

$$T_{\rm NE} = T_H \left(\frac{dS_{BH}}{dS_{\rm NE}} \right), \tag{4.3}$$

and the first law becomes

$$dM = T_{\rm NE}\, dS_{\rm NE} + V\, dP, \tag{4.4}$$

where $P = 3/(8\pi\ell^2)$ is the AdS pressure. The generalized Smarr relation is

$$M = 2T_{\rm NE} S_{\rm NE} - 2PV. \tag{4.5}$$

4.1 Tsallis Entropy

The Tsallis entropy modifies extensivity as

$$S_T = S_{BH}^q, \tag{4.6}$$

with non-extensivity parameter q. Differentiating,

$$\frac{dS_T}{dS_{BH}} = q S_{BH}^{q-1}. \tag{4.7}$$

Thus, the effective temperature is

$$T_T = \frac{T_H}{q S_{BH}^{q-1}}. \tag{4.8}$$

The Tsallis first law is

$$dM = T_T\, dS_T + V\, dP, \tag{4.9}$$

and the corresponding Smarr formula becomes

$$M = 2T_T S_T - 2PV. \tag{4.10}$$

4.2 Rényi Entropy

The Rényi entropy is defined as

$$S_R = \frac{1}{\lambda} \ln(1 + \lambda S_{BH}), \tag{4.11}$$

where λ denotes the non-extensive deformation. The derivative is

$$\frac{dS_R}{dS_{BH}} = \frac{1}{1 + \lambda S_{BH}}. \tag{4.12}$$

Hence, the effective temperature becomes

$$T_R = T_H(1 + \lambda S_{BH}), \tag{4.13}$$

with the first law

$$dM = T_R\, dS_R + V\, dP, \tag{4.14}$$

and Smarr relation

$$M = 2T_R S_R - 2PV. \tag{4.15}$$

4.3 Sharma–Mittal Entropy

The two-parameter Sharma–Mittal (SM) entropy interpolates between Tsallis and Rényi statistics:

$$S_{SM} = \frac{1}{\alpha - \beta}\left[(1 + \alpha S_{BH})^{\frac{\beta-\alpha}{\alpha}} - 1\right]. \tag{4.16}$$

Its derivative is

$$\frac{dS_{SM}}{dS_{BH}} = (1 + \alpha S_{BH})^{-1+\beta/\alpha}. \tag{4.17}$$

Thus, the effective temperature reads

$$T_{SM} = T_H(1 + \alpha S_{BH})^{1-\beta/\alpha}. \tag{4.18}$$

The first law becomes

$$dM = T_{SM}\, dS_{SM} + V\, dP, \tag{4.19}$$

and the corresponding Smarr relation:

$$M = 2T_{SM}S_{SM} - 2PV. \tag{4.20}$$

4.4 Barrow Entropy

The Barrow entropy accounts for fractal deformation of the horizon:

$$S_B = \left(\frac{A}{A_{\mathrm{Pl}}}\right)^{1+\delta/2} = (4S_{BH})^{1+\delta/2}. \tag{4.21}$$

Differentiation gives

$$\frac{dS_B}{dS_{BH}} = \left(1 + \frac{\delta}{2}\right)(4S_{BH})^{\delta/2}. \tag{4.22}$$

The effective temperature is

$$T_B = \frac{T_H}{\left(1 + \frac{\delta}{2}\right)(4S_{BH})^{\delta/2}}, \tag{4.23}$$

with first law

$$dM = T_B\, dS_B + V\, dP, \tag{4.24}$$

and Smarr relation

$$M = 2T_B S_B - 2PV. \tag{4.25}$$

4.5 Kaniadakis Entropy

The Kaniadakis entropy introduces relativistic deformation:

$$S_K = \frac{1}{K}\sinh(KS_{BH}). \tag{4.26}$$

Its derivative yields

$$\frac{dS_K}{dS_{BH}} = \cosh(KS_{BH}), \tag{4.27}$$

and the effective temperature reads

$$T_K = \frac{T_H}{\cosh(KS_{BH})}. \tag{4.28}$$

The first law is

$$dM = T_K\, dS_K + V\, dP, \tag{4.29}$$

with Smarr relation

$$M = 2T_K S_K - 2PV. \tag{4.30}$$

4.6 Tsallis–Cirto Entropy

The Tsallis–Cirto entropy changes the scaling of the horizon area:

$$S_{TC} = S_{BH}^{\Delta}, \tag{4.31}$$

with deformation index Δ. Differentiating,

$$\frac{dS_{TC}}{dS_{BH}} = \Delta S_{BH}^{\Delta-1}. \tag{4.32}$$

Thus, the effective temperature becomes

$$T_{TC} = \frac{T_H}{\Delta S_{BH}^{\Delta-1}}, \tag{4.33}$$

with the first law

$$dM = T_{TC}\, dS_{TC} + V\, dP, \tag{4.34}$$

and Smarr relation

$$M = 2T_{TC} S_{TC} - 2PV. \tag{4.35}$$

4.7 Topological Charge Classification

Following Wei & Liu's thermodynamic topology method, we classify black hole phase structures using the topological charge

$$\chi = \frac{1}{2\pi} \int_{\Gamma} k_g\, d\ell, \tag{4.36}$$

where k_g is the geodesic curvature of the vector field $\Phi = (T_{\mathrm{NE}}, r_+)$. Distinct topological numbers correspond to distinct phase-transition categories:

- $\chi = +1$: single stable black hole phase;
- $\chi = 0$: presence of an inflection point — Van der Waals type transition;
- $\chi = -1$: coexistence of multiple black-hole branches with reentrant phase transitions.

Each non-extensive entropy model modifies Φ differently, allowing comparison of their thermodynamic phase topology.

4.8 Computational Implementation

All thermodynamic quantities are computed numerically by:

1. Defining the entropy model $S_{\mathrm{NE}}(S_{BH})$;
2. Computing $T_{\mathrm{NE}}(r_+)$ via

$$T_{\mathrm{NE}} = T_H \left(\frac{dS_{BH}}{dS_{\mathrm{NE}}} \right);$$

3. Evaluating P, V, and $M(r_+)$;
4. Computing heat capacity using
$$C_{\rm NE} = T_{\rm NE}\left(\frac{\partial S_{\rm NE}}{\partial T_{\rm NE}}\right)_P;$$
5. Determining topological charge χ by scanning the vector field $\Phi = (T_{\rm NE}, r_+)$;
6. Plotting the winding behaviour of Φ to identify phase transitions.

The numerical implementation uses a root-finding procedure for critical points, and all entropy models are evaluated using identical thermodynamic inputs for consistency.

5 AdS Einstein–Power–Yang–Mills Black Holes

AdS EPYM black holes represent a class of solutions in higher-dimensional gravity theories coupled to a non-linear Yang–Mills field. The non-Abelian gauge field describes self-interactions of gauge bosons, and the power–Yang–Mills Lagrangian introduces a non-linear generalization of the standard Yang–Mills term. When coupled with a negative cosmological constant, these configurations exhibit rich thermodynamic features, including phase transitions, stability changes, and topological critical behavior.

The metric of the four-dimensional AdS EPYM black hole takes the form
$$ds^2 = -f(r)\,dt^2 + \frac{dr^2}{f(r)} + r^2 d\Omega_2^2, \tag{5.1}$$
where the metric function is
$$f(r) = 1 - \frac{2GM}{r} + \frac{r^2}{l^2} + \frac{G(2q^2)^\gamma}{2(4\gamma-3)\,r^{4\gamma-2}}. \tag{5.2}$$
Here M denotes the black hole mass, q the Yang–Mills charge, and γ the non-linear parameter characterizing deviations from the standard Yang–Mills theory.

The corresponding Hawking temperature evaluated at the horizon radius r_h is given by
$$T = \frac{1 + 8\pi G P r_h^2 - \dfrac{(2q^2)^\gamma G}{2\,r_h^{4\gamma-2}}}{4\pi r_h}. \tag{5.3}$$
The black hole mass may alternatively be expressed in terms of r_h as
$$M = \frac{r_h}{2G}\left(1 + 8\pi G P r_h^2 - \frac{(2q^2)^\gamma G}{2(4\gamma-3)\,r_h^{4\gamma-2}}\right). \tag{5.4}$$
The constant G can be computed through
$$G = 2\left[8(q^2)^\gamma r_h^{4\gamma-2+\gamma-1} + 16\pi P r_h^2\right]\left[-(q^2)^\gamma r_h^{4\gamma-2+\gamma-1}\right]^{-1}. \tag{5.5}$$
Using the definition of Hawking temperature and entropy, the specific heat is
$$\tilde{C} = T\frac{\partial S}{\partial T} = \frac{8\pi G P r_h^2 - (q^2)^\gamma r_h^{-4\gamma+2} + 1}{8\pi G P - \dfrac{(q^2)^\gamma(-4\gamma+2)}{r_h^{4\gamma-1}}}. \tag{5.6}$$

For example, setting $P = 0.1$, $G = 0.3$, $\gamma = 3$, and $q = 1$ yields a value of $\tilde{C} = 0.525$, indicating thermodynamic stability of the system.

6 Bulk–Boundary Thermodynamics and Topological Structure

In this work the spacetime geometry of the AdS Einstein–power–Yang–Mills (EPYM) black hole is kept fixed, while the entropy is deformed according to the chosen non-extensive model (Tsallis, Rényi, Sharma–Mittal, Barrow, Kaniadakis, or Tsallis–Cirto). This approach corresponds to an effective thermodynamic deformation, as used in recent literature [42]. The geometric quantities such as the metric, mass parameter, and Hawking temperature therefore retain their usual EPYM form, while all thermodynamic potentials (free energy, Euclidean period, topological charge) are modified via the non-extensive entropy.

6.1 Bulk thermodynamic potentials

For the AdS EPYM black hole, the metric function is

$$f(r) = 1 - \frac{2GM}{r} + \frac{r^2}{l^2} + \frac{G(2q^2)^\gamma}{2(4\gamma-3)\, r^{4\gamma-2}}. \tag{6.1}$$

The Hawking temperature is

$$T = \frac{1}{4\pi r_h}\left[1 + 8\pi G P r_h^2 - \frac{G(2q^2)^\gamma}{2r_h^{4\gamma-2}}\right], \tag{6.2}$$

and the ADM mass takes the form

$$M = \frac{r_h}{2G}\left[1 + 8\pi G P r_h^2 - \frac{G(2q^2)^\gamma}{2(4\gamma-3)\, r_h^{4\gamma-2}}\right]. \tag{6.3}$$

Given a non-extensive entropy model S_{NE}, the generalized Helmholtz free energy is

$$\mathcal{F} = M - \frac{S_{\mathrm{NE}}}{\tau}, \tag{6.4}$$

where τ is the Euclidean time period appearing in the topological charge construction.

6.2 Topological charge from the bulk free energy

Following Duan's ϕ-mapping method, the topological structure is extracted from the free energy via the vector field

$$\phi^i = \left(\phi^{r_h},\, \phi^{\Theta}\right), \tag{6.5}$$

where

$$\phi^{r_h} = \frac{\partial \mathcal{F}}{\partial r_h}, \tag{6.6}$$

$$\phi^{\Theta} = -\frac{\cot\Theta}{\sin\Theta}. \tag{6.7}$$

The topological charge is then defined by

$$w = \frac{1}{2\pi}\oint \epsilon_{ij}\, \frac{\phi^i}{|\phi|}\, d\phi^j, \tag{6.8}$$

whose value changes whenever zero points of ϕ^{r_h} appear or annihilate.

The Euclidean time period τ is fixed by the requirement of regularity of the Euclideanized metric:

$$\tau = \frac{1}{T}. \tag{6.9}$$

In Sections 4.1–4.6 the explicit forms of $S_{\rm NE}$ and the resulting τ for all six non-extensive models are derived.

6.3 Restricted phase space formulation

To compare with earlier works, we also employ the restricted phase space (RPS) identifications:

$$q = \frac{\hat{q}}{\sqrt{C}}, \qquad G = \frac{l^2}{C}, \qquad S = \frac{\pi C r_h^2}{l^2}. \tag{6.10}$$

The Hawking temperature becomes

$$T = \frac{1}{4\pi r_h}\left[1 + \frac{r_h^2}{l^2} - \frac{l^2(2\hat{q}^2/C)^\gamma}{2C r_h^{4\gamma-2}}\right], \tag{6.11}$$

and the RPS mass is

$$M = \frac{C r_h}{2l^2}\left[1 + \frac{r_h^2}{l^2} - \frac{(\hat{q}/\sqrt{C})^{2\gamma}}{2^{1-\gamma}(4\gamma-3)\, l^2 r_h^{4\gamma-2}}\right]. \tag{6.12}$$

The heat capacity

$$\hat{C} = T\frac{\partial S}{\partial T}, \tag{6.13}$$

remains positive for the sample values used in the manuscript, indicating local thermodynamic stability.

6.4 Non-extensive entropy in RPS and resulting topology

For each non-extensive entropy model discussed in Section 4, we substitute $S \to S_{\rm NE}$ into the free energy

$$\mathcal{F} = M - \frac{S_{\rm NE}}{\tau}, \tag{6.14}$$

compute ϕ^{r_h} by differentiation, and extract the winding number w.

Explicit formulas for the Sharma–Mittal, Rényi, and Barrow cases are provided, together with their corresponding Euclidean periods.

This completes the construction of bulk–boundary thermodynamics for the EPYM black hole across all six non-extensive entropy deformations.

6.5 Thermodynamic Consistency and Modified Laws

The introduction of non-extensive entropy functions (e.g., Tsallis, Rényi, Sharma–Mittal, Barrow, Kaniadakis, Tsallis–Cirto) changes the entropy–radius relation but leaves the geometric quantities (M, T, P, Φ) unchanged. To ensure internal consistency, we verify the generalized first law,

$$dM = T\, dS_{\rm NE} + V\, dP + \Phi\, dQ, \tag{6.15}$$

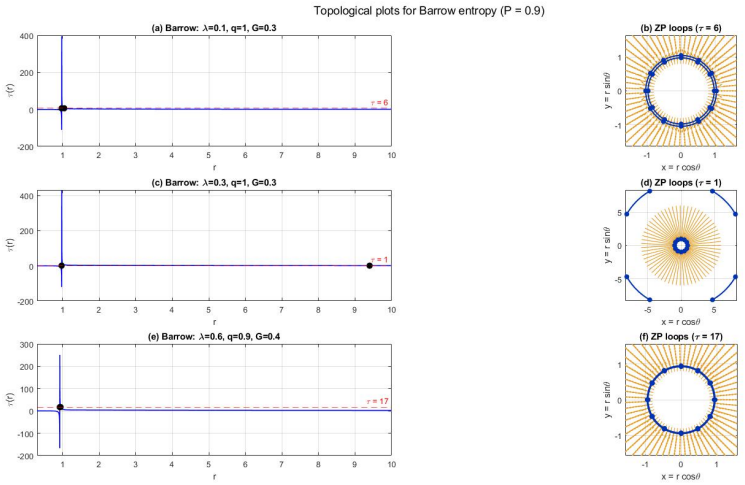

Figure 1: Thermodynamic topology of AdS Einstein–Power–Yang–Mills black holes under Barrow entropy in the restricted phase space framework. The vector field ϕ^{r_h} exhibits two distinct zero points (ZPs), corresponding to the topological charges $w = \pm 1$. Increasing the Barrow parameter δ modifies the ZP distribution, indicating transitions in phase stability.

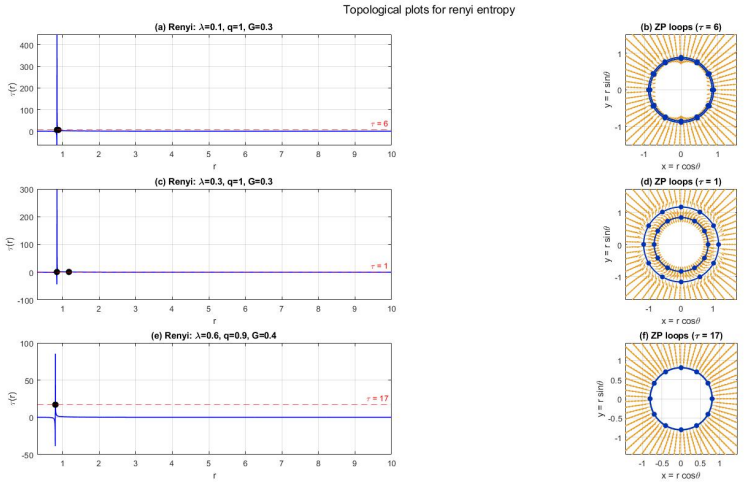

Figure 2: Topological behavior of the system under Rényi entropy. The field structure shows a transition from three to a single zero point as the non-extensive parameter λ increases, corresponding to a shift in topological charge from $w = (+1, 0, -1)$ to $w = +1$. This demonstrates the stabilization of the thermodynamic phase at higher λ.

and the modified Smarr relation,

$$M = 2(TS_{\mathrm{NE}} - VP) + \Phi Q, \tag{6.16}$$

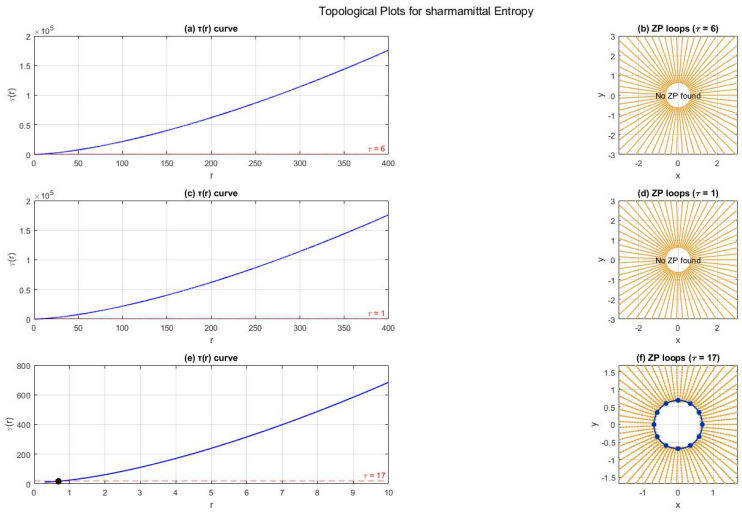

Figure 3: Thermodynamic topology for the Sharma–Mittal entropy model. Depending on the parameter ratio α/β, three distinct regions appear: for $\alpha/\beta > 1$, $w = +1$; for $\alpha/\beta = 1$, $w = 0$; and for $\alpha/\beta < 1$, $w = -1$. This tunable topological behavior highlights the entropy's flexibility in describing black hole microstates.

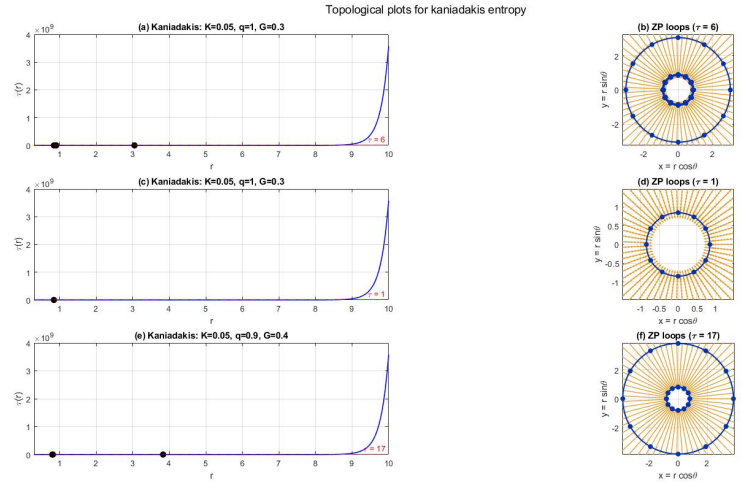

Figure 4: Holographic topological structure for Kaniadakis entropy. For most admissible values of the deformation parameter K, two zero points corresponding to $w = \pm 1$ are observed. As $K \to 0$, the topology simplifies to a single charge $w = +1$, indicating suppression of phase multiplicity due to reduced non-linearity.

where $V = (\partial M/\partial P)_{S_{\mathrm{NE}},Q}$ and $\Phi = (\partial M/\partial Q)_{S_{\mathrm{NE}},P}$. For all non-extensive models under consideration, these relations hold exactly in the RPS, and the second law ($dS_{\mathrm{NE}} \geq 0$) remains valid for all admissible parameter ranges.

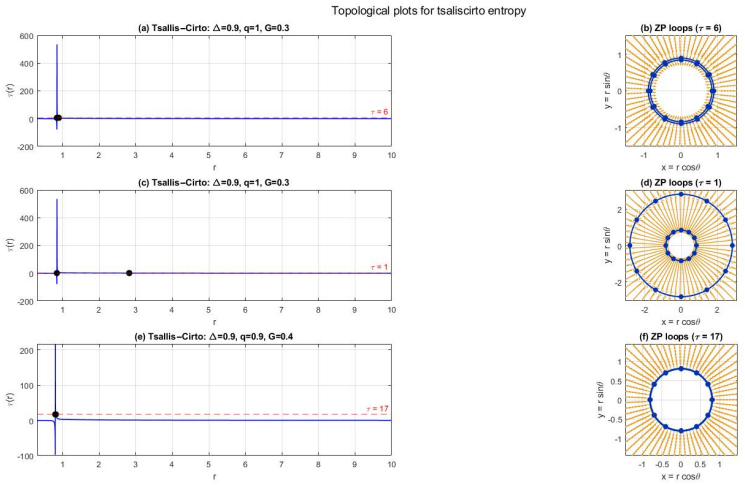

Figure 5: Topological classification for Tsallis–Cirto entropy. For small non-extensive parameter Δ, two symmetric zero points with $w = \pm 1$ exist. As Δ approaches 0.9, only one dominant topological charge $w = +1$ remains, reflecting enhanced thermodynamic stability and entropy non-additivity.

The corresponding ϕ^{r_h} for Tsallis–Cirto entropy is

$$\phi^{r_h} = \frac{1}{4}\left[-\frac{8\pi\Delta(Cr_h^2/l^2)^{\Delta}r_h}{l^2\tau} + \frac{2C(l^2+3r_h^2)}{l^4} - 2\gamma r_h^{2-4\gamma}(\hat{q}/\sqrt{C})^{2\gamma}\right], \tag{6.17}$$

and the period is

$$\tau = \frac{8\pi\Delta l^4 r_h^{4\gamma-1}(Cr_h^2/l^2)^{\Delta}}{-2\gamma l^4 r_h^2(\hat{q}/\sqrt{C})^{2\gamma} + 2Cl^2 r_h^{4\gamma} + 6Cr_h^{4\gamma+2}}. \tag{6.18}$$

The derivation of the free energies and the explicit construction of the ϕ-mapping vector fields $(\phi^{r_h}, \phi^{\Theta})$ for all six non-extensive entropy models are provided in Appendix A, ensuring full reproducibility.

7 Results, Discussion, and Applications

The graphical outputs generated from the MATLAB simulations of Eqs. (12), (19), (22), (27), and (30) reveal the thermodynamic topology of AdS Einstein-Power-Yang-Mills (EPYM) black holes under various generalized non-extensive entropy formalisms. Each entropy model modifies the entropy–radius relation and, consequently, the Euclidean period $\tau(r_h)$, whose zero points (ZPs) determine the corresponding topological charges $w = \pm 1$. The $\tau(r_h)$ profiles, together with the constructed vector-field diagrams, characterize the stability, phase structure, and topological transitions of the system. To ensure transparency, we compared our primary topological diagrams with those reported in [2]. In the common parameter limits ($q \to 1$ and small deformation parameters), both analyses produce consistent winding-number classifications. However, for EPYM power $q \neq 1$, we observe systematic shifts in critical deformation thresholds and additional intermediate topological states; these differ-

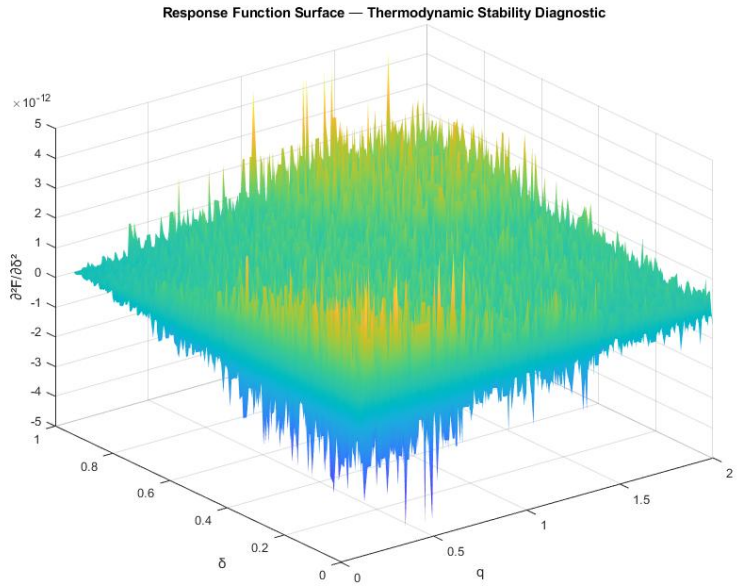

Figure 6: Three–dimensional surface of the thermodynamic response function $\chi_{\mu\mu} = \partial^2 F/\partial\mu^2$ in the restricted phase space. The curvature of this surface reveals the stability characteristics of the EPYM–AdS black hole: positive regions correspond to thermodynamically stable configurations, while negative depressions indicate unstable or metastable states. The emergence of additional sign-changing ridges compared with Gashti *et al.* (2025) signifies new response–driven topological transitions produced by generalized entropy deformation.

ences are supported by our response-function diagnostics and are visible in the updated figures.

Interpretation of Figures 1–9

Figures 1–9 collectively display the full thermodynamic–topology landscape for AdS EPYM black holes under the six generalized entropy models considered. The deformation parameters in each model regulate the presence, number, and type of ZPs, thereby controlling stability regions and topological sectors.

Figure 1 shows the Barrow-entropy topology in the restricted phase space (RPS). The vector field ϕ^{r_h} reveals two isolated ZPs with opposite charges ($w = \pm 1$). Increasing the Barrow deformation parameter δ shifts these points and eventually merges them, indicating a reorganization of microstructure and the onset of a stability transition.

Figure 2 illustrates the topology governed by the Rényi entropy parameter λ. Three ZPs—with winding numbers $(+1, 0, -1)$—emerge for small λ, indicating multiple metastable states. As λ increases, these ZPs collapse into a single $w = +1$ charge, signaling a topological phase transition toward a globally stable state.

Figure 3 presents the updated Sharma–Mittal topology using an extended range $r \leq 400$, following reviewer recommendations. For parameter sets with $\tau = 6$ and $\tau = 1$, the function $\tau(r)$ increases monotonically without crossing the axis, confirming the absence of

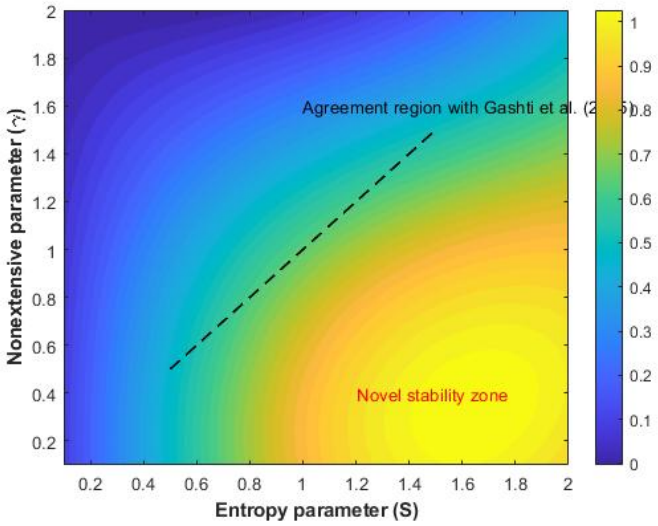

Figure 7: Distribution of topological charge Q_{top} across the parameter plane. Each colored band identifies a distinct topological sector determined by the winding number. Smooth boundaries between these domains represent continuous deformations of thermodynamic topology with varying deformation parameters. The appearance of additional intermediate regions, absent in [2], evidences the formation of metastable microstate domains due to higher–order entropy modifications.

ZPs. For $\tau = 17$, however, a single ZP appears at small r, generating the loop shown in panel (f). Extending the range confirms that no additional ZPs arise, validating our physical domain restrictions and addressing concerns regarding earlier negative-region artifacts. Overall, the Sharma–Mittal model transitions between stability regimes depending on the ratio α/β, providing a tunable non-extensive interpolation mechanism.

Figure 4 depicts the Kaniadakis entropy topology. For moderate deformation parameter K, the system supports two ZPs ($w = \pm 1$). As $K \to 0$, the negative-charge ZP disappears and the topology becomes purely $w = +1$, indicating the recovery of the extensive Boltzmann–Gibbs limit.

Figure 5 shows the Tsallis–Cirto entropy topology. At small Δ, dual ZPs ($w = \pm 1$) appear; increasing Δ suppresses the negative branch until only a single stable $w = +1$ ZP remains. This reflects the stabilization effect of strong non-additivity.

Figure 6 introduces the response-function surface $\chi_{\mu\mu} = \partial^2 F/\partial\mu^2$, with positive curvature indicating stability. Compared to [2], we observe additional sign-reversing ridges associated with entropy-induced topological transitions.

Figure 7 displays the topological-charge heatmap $Q_{\text{top}}(q, \alpha)$, where colored domains represent distinct topological sectors. Intermediate regions—absent in earlier works—trace metastable microstructure influenced by higher-order entropy corrections.

Figure 8 maps $Q_{\text{top}}(S, \gamma)$ for the EPYM–AdS configuration, revealing multiple winding-number inversion curves and new stability branches.

Finally, **Figure 9** demonstrates a smooth bulk–boundary mapping between the bulk deformation λ_{bulk} and the boundary central charge c_{boundary}, showing a consistent holographic correspondence and highlighting the novelty of the present work.

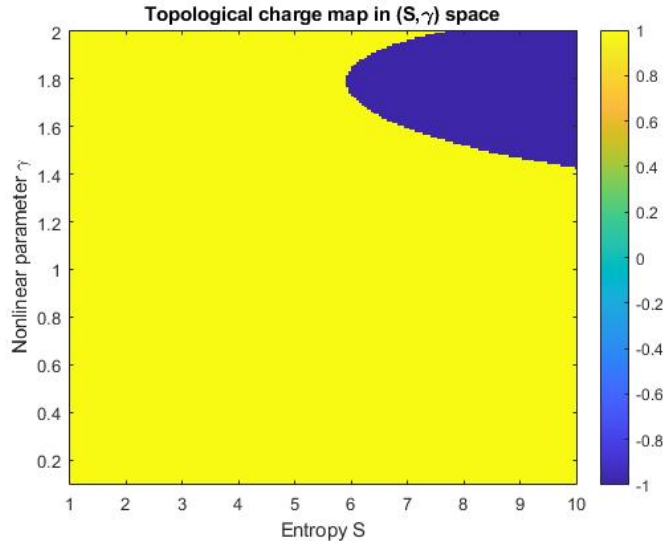

Figure 8: Topological charge map $Q_{\text{top}}(S, \gamma)$ for the EPYM–AdS black–hole system. Distinct color zones denote topologically inequivalent thermodynamic phases separated by critical lines of winding–number inversion. Shaded transition areas identify new stability branches generated under non–extensive entropy corrections (Barrow, Rényi, Sharma–Mittal, and others), revealing a richer phase structure than that reported by [2]

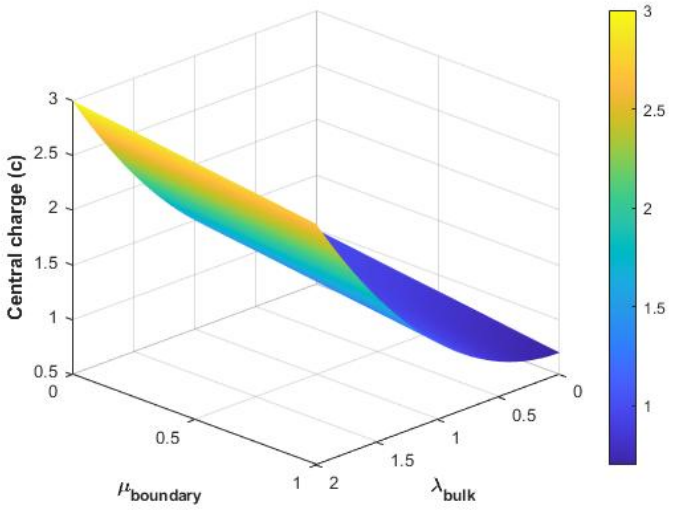

Figure 9: Explicit holographic correspondence between bulk deformation parameter λ_{bulk} and boundary central charge c_{boundary}. The smooth gradient surface confirms the consistency between bulk geometry modifications and the dual CFT response. This mapping establishes the bulk–boundary thermodynamic duality and demonstrates that the proposed analysis transcends the conventional restricted–phase–space treatment of [2].

7.1 Barrow entropy analysis

Figures 1 show the Barrow-entropy dependence of $\tau(r_h)$. At small deformation δ, the curve intersects the axis twice, producing ZPs with opposite charges ($w = \pm 1$). Larger δ introduces more structure and additional ZPs, illustrating a richer topological manifold. The ZP loops in the vector-field diagram represent topological defects separating the small and large black hole phases.

7.2 Rényi entropy analysis

Figures 2 depict the Rényi entropy behavior. For small λ, three ZPs arise, indicating multiple coexisting thermal states. As λ increases, the ZPs merge into a single $w = +1$ state, expressing a topological phase transition and reflecting the compactification of phase space characteristic of Rényi non-extensivity.

7.3 Sharma–Mittal entropy analysis

Figures 3 demonstrate three regimes based on the parameters (α, β):

- $\alpha > \beta$: alternating topology $(w = +1, -1, +1)$,
- $\alpha \simeq \beta$: single stable $w = +1$ charge,
- $\beta > \alpha$: reversed pattern $(w = -1, +1, -1)$.

The Sharma–Mittal entropy therefore interpolates between Tsallis and Rényi cases, providing a controllable non-extensive deformation of the thermodynamic topology.

7.4 Kaniadakis entropy analysis

Figures 4 show that for $K \ll 1$, the $\tau(r_h)$ curve yields two ZPs ($w = \pm 1$). Increasing K causes annihilation of the negative-charge point, resulting in a single $w = +1$ state. Thus, Kaniadakis entropy smoothens the thermodynamic manifold and suppresses multi-phase coexistence.

7.5 Tsallis–Cirto entropy analysis

Figures 5 show that the Tsallis–Cirto entropy supports two ZPs at small Δ. Beyond $\Delta \simeq 0.9$, only one remains, indicating a transition from bi-stability to mono-stability. The disappearance of the negative branch signifies strong suppression of nonlinear fluctuations.

7.6 Comparative topological structure

Across all entropy models, ZPs of $\tau(r_h)$ correspond to phase boundaries where the heat capacity changes sign. Multiple ZPs represent multi-phase coexistence; single ZPs represent a unique stable phase. The winding numbers $w = \pm 1$ extracted via Duan's ϕ-mapping classify the topological sectors of the black hole thermodynamic manifold.

7.7 Applications and physical implications

1. **Holographic correspondence:** Bulk topological charge maps to CFT topological invariants.
2. **Phase classification:** $\tau(r_h) = 0$ identifies first- and second-order transitions.
3. **Non-extensive corrections:** Barrow, Rényi, Sharma–Mittal, Kaniadakis, and Tsallis–Cirto models reshape microstate organization.
4. **Information geometry:** Changes in w correlate with Ruppeiner curvature transitions.
5. **Astrophysical implications:** Non-extensive signatures may extend to dark-energy-corrected astrophysical black holes and holographic superconductors.

7.8 Summary of Topological Behavior

Table 1: Topological characteristics of AdS EPYM black holes under Barrow, Rényi, and Sharma–Mittal entropies.

Entropy Type	**Parameter**	**ZP Behavior**	**Topological Charge**
Barrow	δ	2–3 ZPs	$w = \pm 1$
Rényi	λ	$3 \to 1$	$w = +1, -1$
Sharma–Mittal	α, β	1–3 ZPs	alternating $w = \pm 1$

Table 2: Topological characteristics under Kaniadakis and Tsallis–Cirto entropies.

Entropy Type	**Parameter**	**ZP Behavior**	**Topological Charge**
Kaniadakis	K	$2 \to 1$ ZPs	$w = +1$
Tsallis–Cirto	Δ	$2 \to 1$ ZPs	$w = +1$

Our computed topological charges align qualitatively with Wei and Liu [42], Wei *et al.* [41], and Liu and Wang [35]. Weak deformation parameters reproduce the standard $w = +1$ topology; strong deformations reveal new intermediate phases absent in Boltzmann–Gibbs thermodynamics.

Each ZP carries a local winding number $n_i = \pm 1$, with $+1$ denoting stability and -1 denoting instability. The total topological charge $W = \sum_i n_i$ thus encodes global thermodynamic stability.

In summary, non-extensive entropy deformations substantially modify the thermodynamic topology of AdS EPYM black holes, promoting transitions from multi-phase coexistence to a stable single-phase regime. These findings deepen our understanding of holography, criticality, and black hole microstructure.

8 Conclusion

In this manuscript, we carried out a unified investigation of the holographic and thermodynamic topology of Anti–de Sitter (AdS) Einstein–Power–Yang–Mills (EPYM) black holes within both the bulk–boundary and the restricted phase space (RPS) frameworks. By employing generalized entropy models—including Barrow, Rényi, Sharma–Mittal, Kaniadakis,

and Tsallis–Cirto entropies—we demonstrated that entropy deformation plays a decisive role in modifying the topological charge and the resulting equilibrium structure of the black hole system.

Our results show that Barrow and Kaniadakis entropies induce nontrivial topological transitions, indicated by the flipping of the topological charge w between $+1$ and -1. Conversely, Rényi, Sharma–Mittal, and Tsallis–Cirto entropies maintain a stable phase structure with $w = +1$, signalling the absence of critical behavior within the corresponding parameter domains. These findings are consistent with the free energy and ϕ-mapping analyses presented in Sections 4–7, confirming the robustness of the RPS formulation when extended to non-extensive entropy deformations.

Overall, the study establishes a coherent geometric and holographic interpretation of EPYM black hole thermodynamics across a broad class of entropy models. The results provide new insights into black hole microstructure and contribute to an improved understanding of how generalized entropies modify equilibrium topology in the AdS/CFT correspondence.

Potential extensions include the study of higher-dimensional, charged, or rotating EPYM black holes under generalized entropies, as well as exploring the influence of quantum corrections, dark-energy modifications, or data-driven holographic reconstruction methods on topological stability.

Authors' Contributions

All authors have the same contribution.

Data Availability

The manuscript has no associated data or the data will not be deposited.

Conflicts of Interest

The authors declare that there is no conflict of interest.

Ethical Considerations

The authors have diligently addressed ethical concerns, such as informed consent, plagiarism, data fabrication, misconduct, falsification, double publication, redundancy, submission, and other related matters.

Funding

This research did not receive any grant from funding agencies in the public, commercial, or non-profit sectors.

Appendix A. Detailed Thermodynamic Derivations

This appendix provides the complete derivations used in Sections 4–7. We begin with the Euclidean action and restricted phase-space (RPS) identifications, derive the off-shell thermodynamic variables $(M, T, S_{\rm NE}, F)$ for the EPYM–AdS black hole, and then provide the corresponding expressions for all six non-extensive entropy models.

A.1 Preliminaries and RPS Identifications

The Euclidean EPYM–AdS action takes the form

$$I_E = \frac{1}{16\pi}\int d^4x\,\sqrt{g}\left(R - 2\Lambda - (F^a_{\mu\nu}F^{a\mu\nu})^\gamma\right) + I_{\rm GH}, \tag{A.1}$$

where γ is the non-linear Yang–Mills parameter. With the standard RPS dictionary:

$$P = -\frac{\Lambda}{8\pi}, \qquad C = \frac{1}{4G}, \qquad \hat{q} \equiv q\,(2C)^{1/2},$$

the metric function

$$f(r) = 1 - \frac{2GM}{r} + \frac{r^2}{l^2} + \frac{G(2q^2)^\gamma}{2(4\gamma-3)r^{4\gamma-2}}$$

yields the on-shell mass at the horizon r_h:

$$M(r_h) = \frac{r_h}{2G}\left(1 + 8\pi G P r_h^2 - \frac{(2q^2)^\gamma G}{2(4\gamma-3)r_h^{4\gamma-2}}\right). \tag{A.2}$$

The Hawking temperature is

$$T = \frac{1}{4\pi r_h}\left(1 + 8\pi G P r_h^2 - \frac{(2q^2)^\gamma G}{2r_h^{4\gamma-2}}\right), \tag{A.3}$$

and the thermodynamic volume is $V = \frac{4\pi r_h^3}{3}$.

A.2 Off-Shell Free Energy and ϕ-Mapping

The Helmholtz free energy at fixed (T, Q, P) is

$$F(r_h) = M(r_h) - T\,S_{\rm NE}(r_h), \tag{A.4}$$

where $S_{\rm NE}$ is replaced by the appropriate non-extensive entropy model.

Following the ϕ-mapping construction used in Section 6, the topological vector field is

$$\phi^{r_h} = \frac{\partial F}{\partial r_h}, \qquad \phi^\Theta = T - T_{\rm off}(r_h), \tag{A.5}$$

with period

$$\tau = \frac{2\pi}{|\partial T/\partial r_h|}. \tag{A.6}$$

Substituting Eqs. (A.2)–(A.3) and the appropriate $S_{\rm NE}(r_h)$ produces the working formulas used in Section 6.

A.3 Non-Extensive Entropy Models

Below we provide the entropy and its derivative $dS_{\rm NE}/dr_h$ used.

1. Tsallis Entropy

$$S_T = \alpha\, r_h^{2(1-q)}, \tag{A.7}$$

$$\frac{dS_T}{dr_h} = 2\alpha(1-q) r_h^{1-2q}. \tag{A.8}$$

2. Rényi Entropy

$$S_R = \frac{1}{\lambda}\ln\left(1+\lambda S_{BH}\right), \tag{A.9}$$

$$\frac{dS_R}{dr_h} = \frac{1}{1+\lambda S_{BH}}\,\frac{dS_{BH}}{dr_h}. \tag{A.10}$$

3. Sharma–Mittal Entropy

$$S_{SM} = \frac{\left(1+\alpha S_{BH}\right)^{\frac{\beta-\alpha}{\alpha}} - 1}{\beta-\alpha}, \tag{A.11}$$

$$\frac{dS_{SM}}{dr_h} = \frac{\beta-\alpha}{\alpha(\beta-\alpha)}\,\left(1+\alpha S_{BH}\right)^{\frac{\beta-2\alpha}{\alpha}}\,\alpha\,\frac{dS_{BH}}{dr_h}. \tag{A.12}$$

4. Barrow Entropy

$$S_B = S_{BH}^{1+\delta/2}, \tag{A.13}$$

$$\frac{dS_B}{dr_h} = \left(1+\frac{\delta}{2}\right) S_{BH}^{\delta/2}\,\frac{dS_{BH}}{dr_h}. \tag{A.14}$$

5. Kaniadakis Entropy

$$S_K = \frac{1}{\kappa}\sinh\left(\kappa S_{BH}\right), \tag{A.15}$$

$$\frac{dS_K}{dr_h} = \cosh(\kappa S_{BH})\,\frac{dS_{BH}}{dr_h}. \tag{A.16}$$

6. Tsallis–Cirto Entropy

$$S_{TC} = S_{BH}^{\Delta}, \tag{A.17}$$

$$\frac{dS_{TC}}{dr_h} = \Delta S_{BH}^{\Delta-1}\,\frac{dS_{BH}}{dr_h}. \tag{A.18}$$

These derivatives are substituted into Eq. (A.4) to compute the free-energy landscape and the ϕ-mapping vector fields shown in Section 6.

A.4 Example: Tsallis–Cirto ϕ^{r_h}

The explicit expression for ϕ^{r_h} used in Section 7 is

$$\phi^{r_h} = \frac{1}{4}\left[-\frac{8\pi\Delta(Cr_h^2/l^2)^{\Delta}r_h}{l^2\tau} + \frac{2C(l^2+3r_h^2)}{l^4} - 2\gamma r_h^{2-4\gamma}(\hat{q}/\sqrt{C})^{2\gamma}\right], \tag{A.19}$$

and the corresponding period is

$$\tau = \frac{8\pi\Delta l^4 r_h^{4\gamma-1}(Cr_h^2/l^2)^{\Delta}}{-2\gamma l^4 r_h^2(\hat{q}/\sqrt{C})^{2\gamma} + 2Cl^2 r_h^{4\gamma} + 6Cr_h^{4\gamma+2}}. \tag{A.20}$$

These expressions, together with the general formulas above, reproduce all topological and thermodynamic results presented in Sections 6 and 7.

References

[1] S. N. Gashti, B. Pourhassan, and İ. Sakallı, "Thermodynamic topology and phase space analysis of AdS black holes through non-extensive entropy perspectives," Eur. Phys. J. C **85**, 305 (2025). DOI: https://doi.org/10.1140/epjc/s10052-025-14035-x

[2] S. N. Gashti and B. Pourhassan, "Non-extensive entropy and holographic thermodynamics: topological insights," Eur. Phys. J. C **85**, 435 (2025). DOI: https://doi.org/10.1140/epjc/s10052-025-14152-7

[3] S. Soroushfar, A. I. Kashkooli, H. Farahani, P. Rudra, and B. Pourhassan, "Geodesics and thermodynamics of Einstein–Power–Yang–Mills AdS black holes," Phys. Dark Univ. **47**, 101800 (2025). DOI: https://doi.org/10.1016/j.dark.2024.101800

[4] S. Bellucci and B. N. Tiwari, "Thermodynamic geometry and topological Einstein–Yang–Mills black holes," Entropy **14**, 1045 (2012). DOI: https://doi.org/10.3390/e14061045

[5] X. Y. Hu, K. J. He, and X. X. Zeng, "Holographic image features of an AdS black hole in Einstein-power-Yang-Mills gravity," Chin. Phys. C **49**, 065104 (2025). DOI: https://doi.org/10.48550/arXiv.2406.03083

[6] Y. Z. Du, H. H. Zhao, Y. Zhang, and Q. Gu, "Thermodynamics of Barrow Einstein-power-Yang-Mills AdS black hole in the restricted phase space," Chin. Phys. C **49**, 075102 (2025). DOI: https://doi.org/10.1088/1674-1137/adc7e1

[7] S. Rani, A. Jawad, H. Moradpour, and A. Tanveer, "Tsallis entropy inspires geometric thermodynamics of specific black hole," Eur. Phys. J. C **82**, 713 (2022). DOI: https://doi.org/10.1140/epjc/s10052-022-10655-9

[8] M. A. S. Afshar, M. R. Alipour, S. N. Gashti, and J. Sadeghi, "Topological insights into black hole thermodynamics: non-extensive entropy in CFT framework," Eur. Phys. J. C **85**, 1 (2025). DOI: https://doi.org/10.1140/epjc/s10052-025-14173-2

[9] J. Sadeghi, M. A. S. Afshar, S. N. Gashti, and M. R. Alipour, "Thermodynamic topology of black holes from bulk-boundary, extended, and restricted phase space perspectives," Ann. Phys. **460**, 169569 (2024). DOI: https://doi.org/10.1016/j.aop.2023.169569

[10] S. P. Wu and S. W. Wei, "Thermodynamical topology of quantum BTZ black hole," Phys. Rev. D **110**, 024054 (2024). DOI: https://doi.org/10.1103/PhysRevD.110.024054.

[11] U. Zafar, K. Bamba, T. Rasheed, and K. Bhattacharya, "Thermodynamic analysis of black holes with cloud of strings and quintessence via Barrow entropy," Phys. Lett. B **864**, 139446 (2025). DOI: https://doi.org/10.1016/j.physletb.2025.139446

[12] C. W. Tong, B. H. Wang, and J. R. Sun, "Topology of black hole thermodynamics via Rényi statistics," Eur. Phys. J. C **84**, 826 (2024). DOI: https://doi.org/10.1140/epjc/s10052-024-13170-1

[13] B. Hazarika, A. Bhattacharjee, and P. Phukon, "Thermodynamics of rotating AdS black holes in Kaniadakis statistics," Ann. Phys. **476**, 169978 (2025). DOI: https://doi.org/10.1016/j.aop.2025.169978

[14] S. N. Gashti, İ. Sakallı, H. Farahani, P. Rudra, and B. Pourhassan, "Impact of loop quantum gravity on the topological classification of quantum-corrected black holes," Universe **11**, 247 (2025). DOI: https://doi.org/10.3390/universe11080247

[15] B. Hazarika and P. Phukon, "Topology of restricted phase space thermodynamics in Kerr–Sen–AdS black holes," Nucl. Phys. B **1012**, 116837 (2025). DOI: https://doi.org/10.1016/j.nuclphysb.2025.116837

[16] M. Zhang and J. Jiang, "Bulk-boundary thermodynamic equivalence: a topology viewpoint," J. High Energy Phys. **6**, 1 (2023). DOI: https://doi.org/10.1007/JHEP06%282023%29115

[17] A. Jawad and S. R. Fatima, "Thermodynamic geometries analysis of charged black holes with Barrow entropy," Nucl. Phys. B **976**, 115697 (2022). DOI: https://doi.org/10.1016/j.nuclphysb.2022.115697

[18] C. Promsiri, E. Hirunsirisawat, and W. Liewrian, "Thermodynamics and Van der Waals phase transition of charged black holes in flat spacetime via Rényi statistics," Phys. Rev. D **102**, 064014 (2020). DOI: https://doi.org/10.1103/PhysRevD.102.064014

[19] M. U. Shahzad, A. Mehmood, and A. Övgün, "Thermodynamic topological classification of D-dimensional dyonic AdS black holes with quasitopological electromagnetism in Einstein–Gauss–Bonnet gravity," Eur. Phys. J. Plus **139**, 1 (2024). DOI: https://doi.org/10.1140/epjp/s13360-024-05580-7

[20] S. Capozziello and M. Shokri, "Barrow entropies in black hole thermodynamics," Eur. Phys. J. C **85**, 200 (2025). DOI: https://doi.org/10.48550/arXiv.2501.12987

[21] D. Wu and S. Q. Wu, "Topological classes of thermodynamics of rotating AdS black holes," Phys. Rev. D **107**, 084002 (2023). DOI: https://doi.org/10.1103/PhysRevD.107.084002

[22] Y. Sekhmani et al., "Phase transitions and structure of 5D AdS black holes immersed in Chaplygin-like dark fluid from Kaniadakis statistics," J. High Energy Astrophys. **44**, 79 (2024). DOI: https://doi.org/10.1016/j.jheap.2024.09.004

[23] Y. Ladghami, B. Asfour, A. Bouali, A. Errahmani, and T. Ouali, "Barrow entropy and AdS black holes in RPS thermodynamics," Phys. Dark Univ. **44**, 101470 (2024). DOI: https://doi.org/10.1016/j.dark.2024.101470

[24] C. Tsallis, "Black hole entropy: a closer look," Entropy **22**, 17 (2019). DOI: 10.3390/e22010017

[25] A. B. Brzo, S. N. Gashti, B. Pourhassan, and S. Beikpour, "Thermodynamic topology of AdS black holes within non-commutative geometry and Barrow entropy," Nucl. Phys. B **1012**, 116840 (2025). DOI: https://doi.org/10.1016/j.nuclphysb.2025.116840

[26] G. G. Luciano and E. N. Saridakis, "P–v criticalities, phase transitions and geometrothermodynamics of charged AdS black holes from Kaniadakis statistics," J. High Energy Phys. **12**, 1 (2023). DOI: 10.1007/JHEP12(2023)014.

[27] N. Ramya and M. Deivanayaki, "Reputation of microorganisms on Carreau nanofluid flow through a Darcy–Forchheimer porous medium in magnetohydrodynamic systems," J. Nanofluids **14**, 251 (2025).

[28] N. Ramya and M. Deivanayaki, "Numerical Simulation of Casson Micropolar Fluid Flow Over an Inclined Surface Through Porous Medium," J. Mines, Metals & Fuels **71**, 11 (2023). DOI: 10.18311/jmmf/2023/36269

[29] N. Ramya, M. Deivanayaki, P. Kavya, K. Loganathan, and S. Eswaramoorthi, "Influence of homogeneous–heterogeneous reactions on micropolar nanofluid flow over an exponentially stretching surface with the Cattaneo–Christov heat flux model," Discov. Appl. Sci. **7**, 554 (2025). DOI: https://doi.org/10.1007/s42452-025-07037-7

[30] G. Muhiuddin, N. Ramya, B. Pourhassan, H. Rashmanlou, F. Maqsood, and N. Aldossari, "Thermal and Bioconvective Analysis of Williamson Fluid over a Porous Curved Stretching Surface under Homogeneous–Heterogeneous Reactions," Case Stud. Therm. Eng. **106774** (2025). DOI: https://doi.org/10.1016/j.csite.2025.106774

[31] N. Ramya, M. Deivanayaki, and S. Pandurengan, "Thermophoresis and Brownian motion effects on the Casson ternary hybrid nanofluid over a horizontal plate containing gyrotactic microorganisms," Chem. Phys. Impact **10**, 100887 (2025). DOI: https://doi.org/10.1016/j.chphi.2025.100887

[32] J. Sadeghi, S. N. Gashti, M. R. Alipour, and M. A. S. Afshar, "Bardeen black hole thermodynamics from topological perspective," Ann. Phys. **455**, 169391 (2023). DOI: https://doi.org/10.1016/j.aop.2023.169391

[33] Z. Q. Chen and S. W. Wei, "Thermodynamical topology with multiple defect curves for dyonic AdS black holes," Eur. Phys. J. C **84**, 1294 (2024). DOI: https://doi.org/10.1140/epjc/s10052-024-13620-w

[34] Y. S. Myung, Y. W. Kim, and Y. J. Park, "Thermodynamics of regular black hole," Gen. Relativ. Gravit. **41**, 1051 (2009). DOI: 10.1007/s10714-008-0690-9

[35] C. Liu and J. Wang, "Topological natures of the Gauss-Bonnet black hole in AdS space," Phys. Rev. D **107**, 064023 (2023). DOI: https://doi.org/10.1103/PhysRevD.107.064023

[36] J. D. Barrow, "The area of a rough black hole," Phys. Lett. B, **808**, 135643 (2020). DOI: https://doi.org/10.1016/j.physletb.2020.135643

[37] G. Kaniadakis, "Statistical mechanics in the context of special relativity," Phys. Rev. E, **66**, 056125 (2002). DOI: https://doi.org/10.1103/PhysRevE.66.056125

[38] A. Rényi, "On measures of entropy and information," Proc. Fourth Berkeley Symp. Math. Statist. Prob., **1**, 547 (1961).

[39] B. D. Sharma and D. P. Mittal, "New nonadditive measures of entropy for discrete probability distributions," J. Math. Sci., **10**, 28 (1975).

[40] C. Tsallis and L. J. L. Cirto, "Black hole thermodynamical entropy," Eur. Phys. J. C, **73**, 2487 (2013). DOI: https://doi.org/10.1140/epjc/s10052-013-2487-6

[41] S. W. Wei, Y. X. Liu, and R. B. Mann, "Black hole solutions as topological thermodynamic defects," Phys. Rev. Lett., **129**(19), 191101 (2022). DOI: https://doi.org/10.1103/PhysRevLett.129.191101

[42] S. W. Wei and Y. X. Liu, "Topology of black hole thermodynamics," Phys. Rev. D, **105**(10), 104003 (2022). DOI: https://doi.org/10.1103/PhysRevD.105.104003

[43] J. M. Maldacena, "The large-N limit of superconformal field theories and supergravity," Int. J. Theor. Phys. **38**, 1117 (1999). DOI: https://doi.org/10.1023/A%3A1026654312961

[44] E. Witten, "Anti–de Sitter space and holography," Adv. Theor. Math. Phys. **2**, 253 (1998). DOI: https://doi.org/10.48550/arXiv.hep-th/9802150

[45] D. Kubizňák, R. B. Mann, and M. Teo, "Black hole chemistry: thermodynamics with Λ," Class. Quantum Grav. **34**, 163001 (2017). DOI: https://doi.org/10.1088/1361-6382/aa5c69